Numerical Study of a Research Circulation Control Airfoil Using Navier-Stokes Methods

George D. Shrewsbury*
Lockheed Aeronautical Systems Company, Marietta, Georgia

The compressible Reynolds time-averaged Navier-Stokes equations were used to obtain solutions for flows about a two-dimensional circulation control airfoil. The governing equations were written in conservation form for a body-fitted coordinate system and solved using an alternating direction implicit (ADI) procedure. A modified algebraic eddy viscosity model was used to define the turbulent characteristics of the flow, including the wall jet flow over the Coanda surface at the trailing edge. Numerical results are compared to experimental data obtained for a research circulation control airfoil geometry. Excellent agreement with the experimental results was obtained.

Nomenclature

e = internal energy
k = thermal conductivity
p = pressure
Pr = Prandtl number
$\boldsymbol{q}$ = solution vector
R = gas constant
Re = Reynolds number
t = time
T = static temperature
u = velocity in x direction
v = velocity in y direction
x,y = physical plane coordinates
γ = specific heat ratio
ε = ratio of turbulent to laminar viscosities
ξ,η = transformed plane coordinates
μ = viscosity coefficient
ρ = density
τ = viscous stress tensor components

Introduction

ONE of the most efficient methods for generating increased lift is the circulation control (CC) airfoil. This concept was developed in England[1,2] and introduced into the United States by U.S. Navy researchers.[3–5] It has subsequently been the subject of extensive experimental test programs that have confirmed the high-lift capability of this innovative concept.[6–9] These airfoils obtain lift augmentation by tangentially exhausting a thin jet sheet over a rounded trailing edge with the jet sheet remaining attached well into the airfoil lower surface due to the Coanda effect.

Formerly, analysis methods for CC airfoils[10–13] consisted of computational procedures that used weakly coupled viscous-inviscid procedures to define the complex flowfields resulting from the presence of the jet sheet exhausting into the trailing-edge region. Particularly good results were obtained by using a potential flow CC airfoil solver developed by Dvorak et al.[11,13] coupled with a parabolized Navier-Stokes wall-jet analysis program written by Dash and associates.[12]

The complex flowfields of the CC airfoil are governed by highly interactive flow regimes, however, and a comprehensive analysis of the flowfield and the associated phenomena, including the effects of jet entrainment and Coanda surface geometry, requires analysis procedures that account for the strongly coupled nature of the viscous and inviscid flow regimes.

Recently, Navier-Stokes methods have been used successfully to solve for the aerodynamics about CC airfoils.[14–17] The purpose of this paper is to present the results obtained by using the method developed in Ref. 15 to correlate numerical results with performance data from an extensive experimental study.[18] This method solves the fully elliptic Navier-Stokes equations in two-dimensional planar coordinates. The mathematical and numerical formulations are discussed and appropriate boundary conditions and grid generation procedures are defined. Modifications to existing eddy viscosity turbulence models to account for curved wall jets are discussed.

Method

Mathematical Formulation

The development of the two-dimensional, unsteady, compressible Navier-Stokes equations used for this study are documented in Ref. 19 and refinements to the method are reported in Refs. 20–22.

The compressible Reynolds time averaged Navier-Stokes equations may be written in vector form as follows:

$$\frac{\partial}{\partial\tau}[\hat{q}]+\frac{\partial}{\partial\xi}[\hat{F}]+\frac{\partial}{\partial\eta}[\hat{G}]=\frac{1}{Re}\left\{\frac{\partial}{\partial\xi}[\hat{F}_1]+\frac{\partial}{\partial\eta}[\hat{G}_1]\right\} \quad (1)$$

where ξ, η, and τ are the independent variables subject to the general transformation

$$\xi=\xi(x,y,t)$$
$$\eta=\eta(x,y,t)$$
$$\tau=t \quad (2)$$

$$[\hat{q}]=(1/J)[\boldsymbol{q}]$$
$$[\hat{F}]=(1/J)[\xi_t\boldsymbol{q}+\xi_x\boldsymbol{F}+\xi_y\boldsymbol{G}]$$
$$[\hat{G}]=(1/J)[\eta_t\boldsymbol{q}+\eta_x\boldsymbol{F}+\eta_y\boldsymbol{G}]$$
$$[\hat{F}_1]=(1/J)[\xi_x\boldsymbol{F}_1+\xi_y\boldsymbol{G}_1]$$
$$[\hat{G}_1]=(1/J)[\eta_x\boldsymbol{F}_1+\eta_y\boldsymbol{G}_1] \quad (3)$$

Presented as Paper 87-0002 at the AIAA 25th Aerospace Sciences Meeting, Reno, NV, Jan. 12-15, 1987; received April 5, 1987; revision received June 1, 1988.

*Advanced Flight Sciences Department. Member AIAA.

where

$$q=\begin{Bmatrix}\rho\\ \rho u\\ \rho v\\ \rho e\end{Bmatrix}\quad F=\begin{Bmatrix}\rho u\\ \rho u^2+p\\ \rho uv\\ (\rho e+p)u\end{Bmatrix}$$

$$G=\begin{Bmatrix}\rho v\\ \rho uv\\ \rho v^2+p\\ (\rho e+p)v\end{Bmatrix}\quad F_1=\begin{Bmatrix}0\\ \tau_{xx}\\ \tau_{xy}\\ \frac{\gamma}{Pr}k\frac{\partial e}{\partial x}+u\tau_{xx}+v\tau_{xy}\end{Bmatrix}$$

$$G_1=\begin{Bmatrix}0\\ \tau_{xy}\\ \tau_{yy}\\ \frac{\gamma}{Pr}k\frac{\partial e}{\partial y}+u\tau_{xy}+v\tau_{yy}\end{Bmatrix} \tag{4}$$

The components of the viscous stress tensor are given by

$$\tau_{xx}=\frac{4}{3}\frac{\partial u}{\partial x}-\frac{2}{3}\frac{\partial v}{\partial y}$$

$$\tau_{yy}=\frac{4}{3}\frac{\partial v}{\partial y}-\frac{2}{3}\frac{\partial u}{\partial x}$$

$$\tau_{xy}=(1+\varepsilon)\left(\frac{\partial u}{\partial y}+\frac{\partial v}{\partial x}\right) \tag{5}$$

The equation of state $p=\rho RT$ is required for closure of the system of equations.

In the aforementioned equations, all distances are normalized with respect to the airfoil chord, the velocities are normalized with respect to the freestream velocity V_∞, the density is normalized with respect to the freestream density, and the specific internal energy is normalized with respect to V_∞^2.

Numerical Formulation

The numerical procedure used to solve the system of governing equations is a modified form of the Briley-McDonald[23] alternating direction implicit (ADI) procedure, which is based on the Douglas-Gunn[24] method. It is also closely related to the Warming-Beam[25] algorithm. Variable time steps and numerical dissipation have been incorporated to accelerate the convergence for steady-state flow problems.

The method can be outlined as follows. The governing equations are parabolic with respect to time. Assuming the flowfield is known at a time level t^n, the numerical procedure is used to advance the solution to a new time level t^{n+1} using a fairly large time step. If a steady-state solution is desired, the procedure at each cell is advanced at a different time step based on the local cell Reynolds number. The mixed derivatives that arise from terms such as $(\xi_x u\tau_{xx})_\xi$, etc., are lagged one time step. The flow quantities ρ, u, v, and e at the new time level are written in terms of their values at the known time level and the incremental quantities; i.e.,

$$\rho^{n+1}=\rho^n+\Delta\rho^n$$

The nonlinear terms involved are linearized by using a Taylor expansion about the solution at the known time level t^n. Performing these operations and taking all the known quantities to the right-hand side, one obtains a linear system of equations for the incremental quantities at each grid point in the computational plane, excluding the boundaries. The difference equations may be written in matrix form as

$$[A]\{\Delta q\}^n+\frac{\partial}{\partial\xi}[B]\{\Delta q\}^n+\frac{\partial}{\partial\eta}[C]\{\Delta q\}^n=[R]^n \tag{6}$$

The Douglas-Gunn procedure for generating an ADI scheme is used to solve the above system of equations by approximate factorization of Eq. (6) into two equations, where each involves only a one-dimensional operator

$$[A]\{\Delta q\}^*+\frac{\partial}{\partial\xi}[B]\{\Delta q\}^*=\{R\}^n \tag{7}$$

$$[A]\{\Delta q\}^n+\frac{\partial}{\partial\eta}[C]\{\Delta q\}^n=[A]\{\Delta q\}^* \tag{8}$$

where

$$\{\Delta q\}=\{\Delta\rho,\Delta u,\Delta v,\Delta e\}^\tau \tag{9}$$

Equations (7) and (8) are discretized using second-order accurate difference formulas for the spatial derivatives. This technique results in a matrix system with a block tridiagonal structure that may be solved efficiently by using standard block elimination procedures. The boundary conditions for the unknown vector $\{\Delta q\}$ are evaluated explicitly. Once $\{\Delta q\}^n$ is obtained, the flowfield variables at the new time level are explicitly known.

Artificial Dissipation Terms

To suppress the high-frequency components that appear in regions containing severe pressure gradients (i.e., the neighborhood of shock waves or stagnation points), artificial dissipation terms have been added in conservative form. In the present application, a blend of second- and fourth-order terms with coefficients that depend on the magnitude of the local pressure gradient have been added explicitly for each dependent variable in the manner suggested by Jameson et al.[26] and second-order dissipation terms have been added implicitly for each of the independent variables. The coefficients of the implicit terms were added in the manner suggested by Steger.[27] Extensive numerical experiments have shown that the blending of the dissipation terms provided better shock wave prediction with controlled overshoot pressure distribution.

Turbulence Model

An algebraic eddy viscosity model developed by Baldwin and Lomax[28] was used to define the turbulence transport everywhere except in the wall jet free shear layer. This model permits the calculation of the turbulence characteristics of the boundary layer by defining a two-layer system. The viscosity in the inner layer is given by simple mixing length theory, where the length scale is proportional to the distance from the wall multiplied by the van Driest damping term and the velocity scale is proportional to the length multiplied by the absolute value of the vorticity

$$\mu_{t_{\text{inner}}}=\rho l^2|\omega| \tag{10}$$

where

$$l=ky[1-\exp(-y^+/A^+)] \tag{11}$$

In the outer layer, the velocity and length scales are constant and the turbulent viscosity is calculated from

$$\mu_{t_{\text{outer}}}=KC_{\text{cp}}\rho F_{\text{wake}}F_{\text{kleb}} \tag{12}$$

F_{wake} is defined as the minimum value of

$$y_{\max}F_{\max}$$

or

$$C_{\text{wk}}Y_{\max}U_{\text{diff}}^2/F_{\max}$$

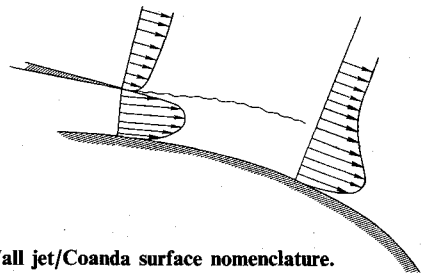

Fig. 1 Wall jet/Coanda surface nomenclature.

F_{max} is determined from the maximum value of

$$F(y) = y|\omega|\,[1 - \exp(-y^+/A^+)]$$

and y_{max} is defined as the y at which F_{max} occurs. F_{kleb} and U_{diff} are defined by

$$F_{kleb} = \left[1 + 5.5\left(\frac{C_{kleb}\, y}{y_{max}}\right)^6\right]^{-1}$$

$$U_{diff} = (\sqrt{u^2+v^2})_{max} - (\sqrt{u^2+v^2})_{min}$$

The constants used in these equations are defined in Ref. 28.

The division between the inner and outer layers is taken as that point at which

$$\mu_{t_{outer}} = \mu_{t_{inner}}$$

The turbulence characteristics of the curved wall jet on the Coanda surface require special treatment, since the extra rates of strain produced by the curvature can exert an influence on the turbulence structure by augmenting or suppressing radial velocity fluctuations. In a curved wall jet, such as that shown in Fig. 1, a balance of centrifugal and pressure forces on a fluid element reveals that increases in velocity with distance from the center of streamline curvature generate stable flows, while flows in which the velocity decreases from the center of curvature are destabilized.[29] In turbulent flow, these stabilities and instabilities lead to an increase or decrease in turbulent transport. This influence can result in viscosities that are an order of magnitude greater than those obtained in planar flows.[30] Accordingly, turbulence models using standard eddy viscosity relations will require significant empirical modifications to reproduce the characteristics of curved shear layer flows. For this study, the mixing length was multiplied by an empirical curvature correction

$$F = 1 - \alpha S$$

where α is an empirical constant whose value depends on the particular flow considered. A review of the literature suggests that most researchers place the constant in the range $6 < \alpha < 14$ for wall-bounded flows. For this study, however, a value of 25 produced results more nearly in agreement with experimental data. A dimensionless parameter S is representative of the ratio of the extra rate of strain produced by the curvature to the inherent shear strain,

$$S = \frac{U/r}{\partial U/\partial n}$$

where U is the velocity in the streamwise direction, n the normal direction, and r the local radius of curvature of the streamline considered. In areas where the curvature is small to moderate, the correction to the eddy viscosity is negligible.

The location of the wake was approximated by determining the point, nearest the trailing edge, at which the U component of the contravariant velocity at the second grid line changed direction. The wake was then arbitrarily defined to exist in the region contained in the four grid points on each side of that location. The calculation of the eddy viscosity began at the lower edge of the wake and proceeded clockwise to the upper edge of the wake. Values of the turbulent viscosity for the wake were then interpolated linearly from the values at the wake edges.

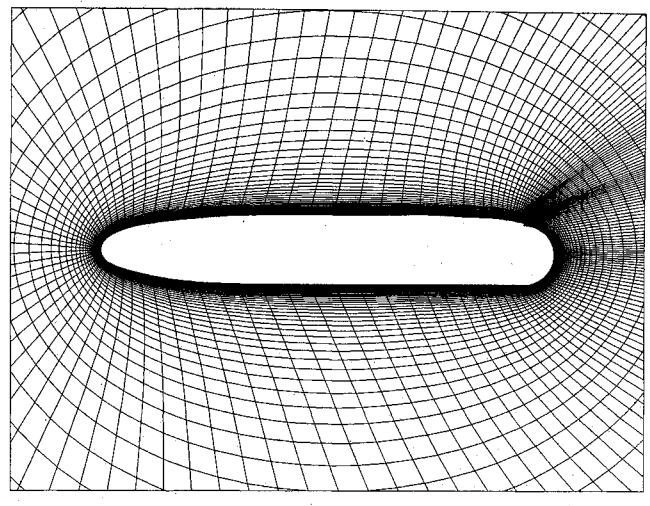

Fig. 2 Computational grid.

Grid Generation and Boundary Conditions

A body-fitted coordinate system is desired for numerical analysis procedures, since boundary surfaces in the physical plane are mapped onto rectangular surfaces in the transformed plane and the boundary conditions in the transformed plane may be treated more accurately. Computer methods developed by Thomas[31] were employed to generate a suitable body-fitted, curvilinear grid system. This procedure uses a Poisson solver to define two-dimensional grids about airfoils and other shapes.

The unique trailing-edge geometry and flow characteristics of CC airfoils makes the use of conventional C-grids difficult, since it is impossible to locate the cut line so that it corresponds to the physical location of the wake. Consequently, it was decided to use an O-grid topology for this analysis. This choice represents a compromise between suitable resolution on the Coanda surface and adequate definition in the near-wake region.

The grid spacing in the direction normal to the airfoil surface was sufficiently dense to permit satisfactory resolution of the boundary layer. In this direction, grid lines were used and approximately 20 of these were submerged in the boundary layer. The grid spacing in the normal direction varied from 0.00007 chords at the wall to 0.60 chords at the outer boundary. The outer boundary was defined as circular and was 14 chords in diameter. In the wraparound direction, 151 points were used. Grid points were clustered to permit satisfactory resolution at critical locations, such as the leading edge and blowing slot exit planes. One of the computational grids used for this study is shown in Fig. 2.

Boundary conditions for the computational plane consisted of specifying the flow conditions along the airfoil surface, including the blowing slot exit plane, the O-grid cut line, and the outer boundary. On the airfoil surface, an adiabatic wall condition $\partial e/\partial \eta = 0$ was imposed and extrapolated values of density were specified. A no-slip condition ($u = v = 0$) was used to define the velocities. At the slot blowing exit, specified values of total pressure and total temperature were used with an extrapolated value of pressure to define the boundary characteristics. Along the grid cut line, boundary conditions were applied explicitly as the average of the extrapolated values from each direction.

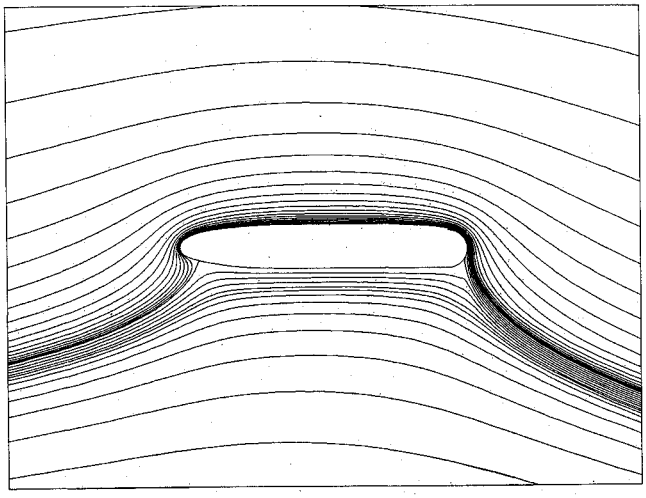

Fig. 3 Computed streamlines for research CC airfoil.

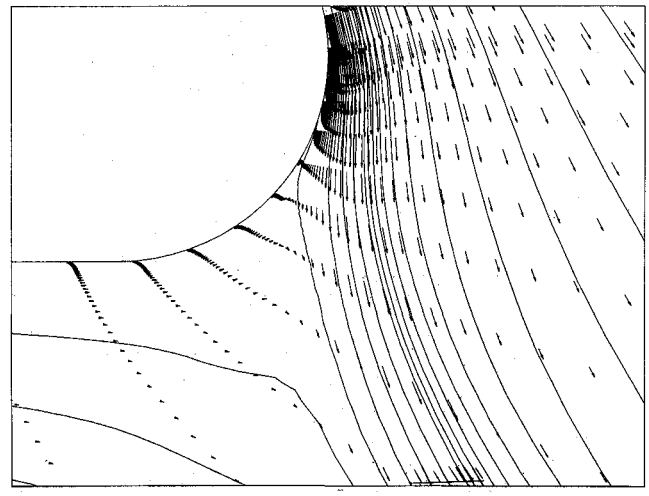

Fig. 4 Computed velocity vectors and streamlines.

At the outer boundary, conditions were applied according to the rule that flow variables should be extrapolated along characteristics leaving the cell and specified along characteristics entering the cell. Accordingly, for subsonic conditions where the boundary is experiencing inflow, values of the velocity and pressure are specified, while the energy is extrapolated from the interior. For outflow conditions, the pressure is specified, while values of velocity and energy are extrapolated from the interior. Numerical disturbances generated by the body may be reflected back into the computational plane, creating an adverse influence on the convergence characteristics of the solution. To eliminate the reflection of unwanted propagations, the pressure is specified according to nonreflecting boundary criteria prescribed by Rudy and Strikwerda,[32] which have been implemented at the outflow boundaries.

In all cases where extrapolated values were specified at the boundaries, a two-point extrapolation of the form

$$q_1 = (4/3)\, q_2 - (1/3)\, q_3$$

was used.

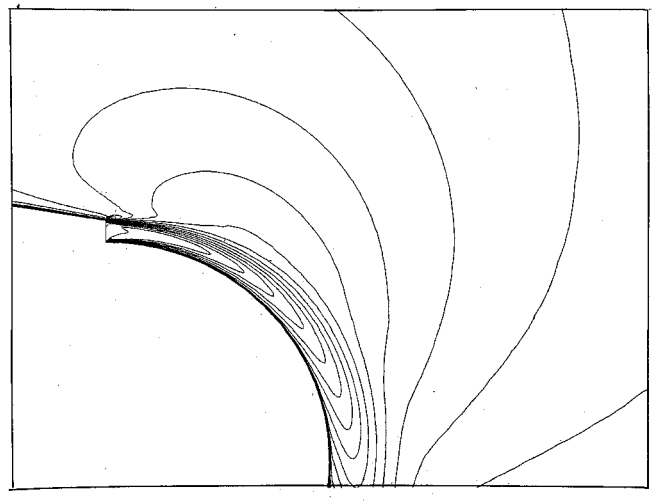

Fig. 5 Computed lines of constant pressure.

Results

Novak and Cornelius[18] conducted wind-tunnel tests on a 15.6% thick CC airfoil section that had been specifically designed to provide data for Navier-Stokes code validation. The blowing slot height-to-radius ratio was 0.1 and the overall chord length was 15 in. This model was designed with a cylindrical Coanda surface with a radius-to-chord ratio of 0.067. While this ratio is relatively high and is certainly not representative of practical flight systems, it does provide a physically large slot height, which improves the quality of the measurements. Data were acquired in the Lockheed-Georgia Low Turbulence Wind Tunnel at a freestream Mach number of 0.0853 and a Reynolds number of 780,000. The model angle of attack was 0 deg. The data consisted of airfoil surface pressure measurements and extensive flowfield surveys using a laser velocimeter (LV). An extension to this experimental effort was performed with a smaller slot height and lower jet momentum coefficients. This work is reported in Ref. 33. The general profile of the section used to obtain these data can be visualized from the grid shown in Fig. 2.

Once a suitable computational grid had been constructed, numerical studies were conducted at a Mach number and Reynolds number corresponding to the experimental tests. The angle of attack was varied numerically until a lift coefficient based on integrated pressures was obtained that corresponded to the experimental zero incidence case.

Angle-of-attack corrections for wind-tunnel data obtained for large values of lift coefficient can be significant because of the wall interference effects encountered when high circulation is present. Circulation control airfoil performance data from Ref. 34, for example, show angle-of-attack corrections approximately equal to $-\frac{2}{3}$ times the lift coefficient. In view of the high lift coefficients produced by circulation control airfoils, the 2 deg correction required for correlation with the wind-tunnel data seems appropriate.

The numerical results were obtained by executing the code on the Lockheed/ASG Cray X-MP/24 computer. Approximately 1000 iterations were required to obtain a converged, steady-state solution. This formulation of the Navier-Stokes equations requires approximately 2.5×10^{-4} CPU s/grid point/time step of Cray execution time.

The computed data presented in Figs. 3–5 were obtained for a jet total pressure ratio of 1.10. The ratio of jet total temperature to freestream total temperature was 0.964. The numerical angle of attack was −2.00 deg and the corresponding lift coefficient was 4.55.

Computed streamlines for the research airfoil are shown in Fig. 3. This figure clearly demonstrates the characteristic flows for CC airfoils, including the large, induced circulation that produces a strong downwash in the wake region and upwash

at the leading edge. The jet entrainment effects on the upper surface and the Coanda turning of the jet can also be seen.

Computed velocity vectors and streamlines in the trailing-edge region are shown for the same case in Fig. 4. The jet flow momentum coefficient for this condition was 0.275. Details of the wall jet development, as well as the interaction of the upper and lower surface flows, can be clearly visualized. These results demonstrate the attached, well-behaved nature of the flow at high values of momentum coefficient.

Lines of constant Mach number in the region of the jet and Coanda turning surface are shown in Fig. 5. The jet flow momentum coefficient was the same as the previous case. The maximum local Mach number was approximately 0.5. The initial acceleration of the flow, and then the systematic decay of the Mach number as the flow progresses, can be observed. In addition, the effects of entrainment of external flow at the jet outer boundary can be seen. At the confluence of the external and jet flows, the external flow near the jet is accelerated by viscous diffusion of the jet momentum.

Computed velocity vectors in the jet and trailing-edge region for a similar condition and configuration are shown in Fig. 6. The geometry for this case is identical to the previous cases, except that the slot height is reduced. The jet total pressure ratio was 1.08 and the corresponding jet momentum coefficient was 0.036. The corresponding lift coefficient was 1.50. The jet sheet detaches much earlier for this condition and the existence of a complex, counter-rotating vortex pair can be seen. The lower vortex does not extend to the Coanda surface. Instead, some flow from the lower surface passes between the wall and the vortex and experiences some acceleration between the two vortex structures, before decelerating and turning near the jet sheet detachment point.

Computed streamlines for this same condition are compared to experimentally obtained results from Ref. 33 in Fig. 7. Lines of constant stream function for the computed case are shown in Fig. 7a and for the experimental study in Fig. 7b. The experimental streamlines were obtained by circumferential interpolation of a comprehensive array of LV data and then integrating radially to obtain values of stream function. Some of the lines of constant stream function from the computations are slightly erratic from interpolation errors, but the overall nature of the flow can, nevertheless, still be visualized. Both the numerical and experimental cases had a lift coefficient of 1.5, but the experimental study was performed at a slightly lower jet momentum coefficient of 0.030.

The most significant discrepancy between the computed and experimental results is that the lower vortex structure in the experimental data is attached to the Coanda surface. In addition, a limiting, stagnation streamline divides the two vortices. The similarity between the computed and experimental flows, however, is striking. The most notable common characteristic is the existence of the "hump" in the jet detachment streamline, which occurs as the flow passes over the upper vortex structure.

Several factors may be considered to account for the differences in the lower vortex characteristics: 1) flows of this nature generally exhibit highly unsteady behavior—the computed results represent an instantaneous picture of that unsteady flow, while the experimental results are a time-averaged representation of the flow; 2) the lower vortex is in a region of lower energy when compared to the upper vortex and, consequently may be much more susceptible to inadequacies in turbulence modeling; and 3) the computed results may represent a bifurcated solution obtained from improper or arbitrary initial conditions.

Experimental and computed CC airfoil pressure distributions are compared in Fig. 8 for the 4.55 lift coefficient case. The agreement between the experimental and numerical pressure distributions is very good. The strong suction peaks produced by the supercirculation at the leading edge and the jet sheet turning on the Coanda surface are very accurately predicted. The discrepancy between the computed and experimental data on the lower surface, near the trailing edge, is probably the result of differences in the locations of the jet sheet detachment points, as observed experimentally and predicted numerically.

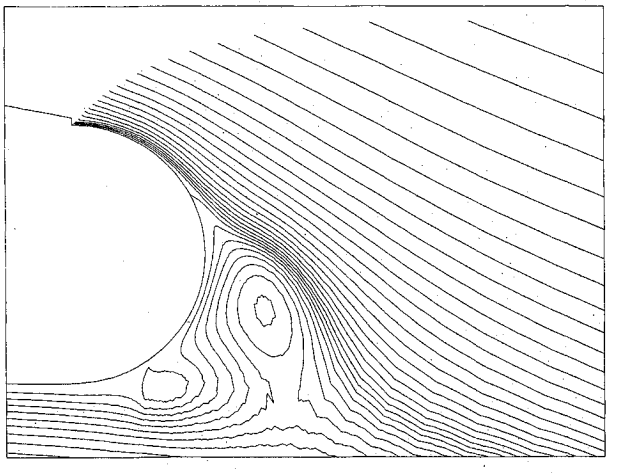

Fig. 7a Computed streamlines, $C_\mu = 0.036$.

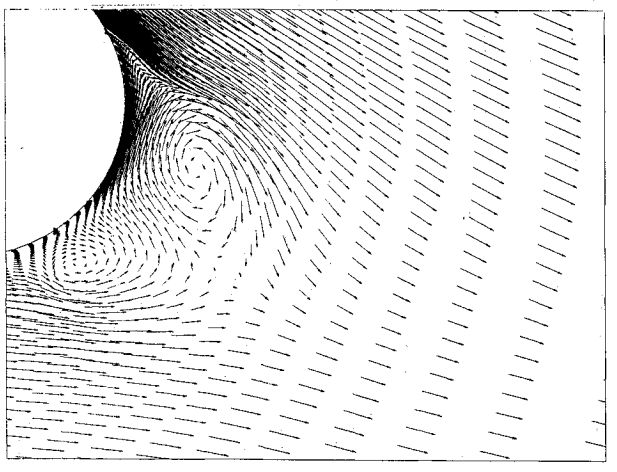

Fig. 6 Computed velocity vectors, $C_\mu = 0.036$.

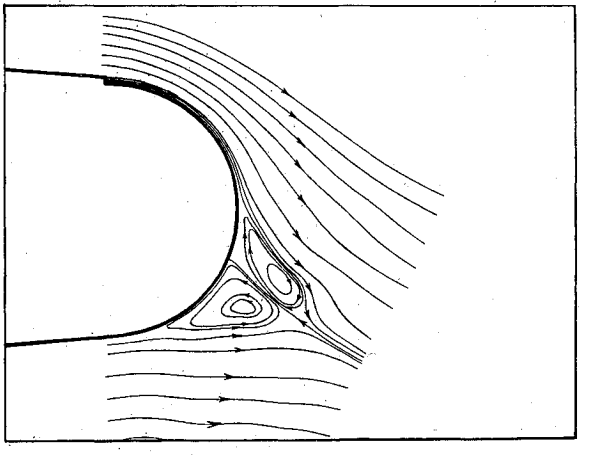

Fig. 7b Experimental streamlines.

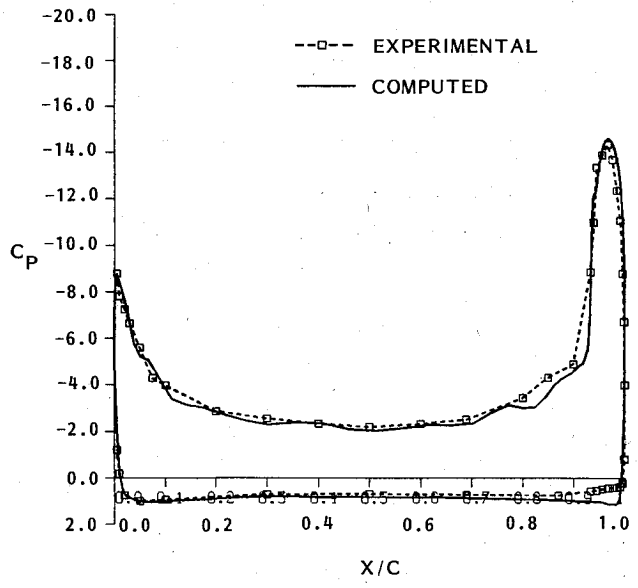

Fig. 8 Computed and experimental pressure coefficient distributions.

Conclusions

A computational procedure has been developed that permits the calculation of the performance characteristics of circulation control airfoils over a broad range of freestream conditions. The fully elliptic, Reynolds time-averaged, Navier-Stokes equations were solved numerically, using an alternating direction implicit (ADI) algorithm. The computed results compared well with experiments conducted on a research circulation control (CC) airfoil that had been specifically designed to provide data for Navier-Stokes code validation, including force data and detailed flow measurements taken in the trailing-edge region. A specially modified algebraic eddy viscosity model was used to predict the behavior of the wall jet and, although the overall behavior of the curved wall jet was sufficiently approximated, important turbulent characteristics crucial to the prediction of the jet sheet detachment point were not adequately predicted. Extensions to the present work will include the incorporation of advanced turbulence models to provide improved analysis of the wall jet characteristics.

References

[1]Cheeseman, I. C. and Seed, A. R., "The Application of Circulation Control by Blowing to Helicopter Rotors," *Journal of the Royal Aeronautical Society*, Vol 71, July 1966.

[2]Kind, R. J., "A Calculation Method for Circulation Control by Tangential Blowing Around a Bluff Trailing Edge," *Aeronautical Quarterly*, Vol. XIX, Aug. 1968, pp. 205–233.

[3]Williams, R. M., "Some Research on Rotor Circulation Control," *Proceedings of the Third Cal/AVLABS Symposium*, Vol. 11, June 1969.

[4]Williams, R. M. and Howe, H. J., "Two-Dimensional Subsonic Wind Tunnel Tests on a 20% Thick, 5% Cambered Circulation Control Airfoil," NSRDC TN AL-176, Aug. 1970.

[5]Englar, R. J., "Two-Dimensional Transonic Wind Tunnel Tests of Three 15-Percent Thick-Circulation Control Airfoils," NSRDC Rept. ASED-182, Dec. 1970.

[6]Abramson, J. and Rogers, E. O., "High-Speed Characteristics of Circulation Control Airfoils," AIAA Paper 83-0265, Jan. 1983.

[7]Loth, J. L. and Boasson, M., "Circulation Controlled STOL Wing Optimization," AIAA Paper 83-0082, Jan. 1983.

[8]Wood, N. J., "The Performance of a Circulation Control Airfoil at Transonic Speeds," AIAA Paper 83-0083, Jan. 1983.

[9]Englar, R. J. and Huson, G. G., "Development of Advanced Circulation Control Wing High Lift Airfoils," AIAA Paper 83-1847, July 1983.

[10]Gibbs, E. H. and Ness, N., "Analysis of Circulation Controlled Airfoils," Dept. of Aerospace Engineering, West Virginia Univ., Morgantown, Rept. TR-43, June 1975.

[11]Dvorak, F. A. and Kind, R. J., "Analysis Method for Viscous Flow Over Circulation-Controlled Airfoils," *Journal of Aircraft*, Vol. 16, Jan. 1979.

[12]Dash, S. M. and Wolf, D. E., "Viscous/Inviscid Analysis of Curved Wall Jets: Part 1—Inviscid Shock Capturing Model (SCIPWJET)," SAI/PR TR-5, Sept. 1982.

[13]Dvorak, F. A. and Choi, D. H., "Analysis of Circulation Controlled Airfoils in Transonic Flow," *Journal of Aircraft*, Vol. 20, April 1983.

[14]Shrewsbury. G., "Numerical Evaluation of Circulation Control Airfoil Performance Using Navier-Stokes Methods," AIAA Paper 86-0286, Jan. 1986.

[15]Shrewsbury, G. D., "Analysis of Circulation Control Airfoils Using an Implicit Navier-Stokes Solver," AIAA Paper 85-0171, Jan. 1985.

[16]Berman, H. A., "A Navier-Stokes Investigation of a Circulation Control Airfoil," AIAA Paper 85-0300, Jan. 1985.

[17]Pulliam, T. H., Jesperson, D. C., and Barth, T. J., "Navier-Stokes Computations for Circulation Controlled Airfoils," AIAA Paper 85-1587, July 1985.

[18]Novak, C. J. and Cornelius, K. C., "An LDV Investigation of a Circulation Airfoil Flowfield," AIAA Paper 86-0503, Jan. 1986.

[19]Tassa, Y., "An Implicit Method for Solving the Navier-Stokes Equations with Application to Shock Boundary Layer Interaction," Lockheed-Georgia, Rept. LG79RR001, 1979.

[20]Sankar, N. L. and Tassa, Y., "Reynolds Number and Compressibility Effects on Dynamic Stall of a NACA 0012 Airfoil," AIAA Paper 80-0010, Jan. 1980.

[21]Shrewsbury, G. D. and Tassa, Y., "Numerical Simulation of Transonic Flow About Isolated Afterbodies," AIAA Paper 83-0498, Jan. 1983.

[22]Schuster, D. M. and Birckelbaw, L. D., "Numerical Computation of Viscous Flowfields about Multiple Component Airfoils," AIAA Paper 85-0167, Jan. 1985.

[23]Briley, W. R. and McDonald, H., "An Implicit Numerical Method for Multidimensional Compressible Navier-Stokes Equations," United Aircraft Research Labs., East Hartford, CT, Rept. M9113363-6, Nov. 1973.

[24]Douglas, J. and Gunn, J. E., "A General Formulation of Alternating Direction Methods," *Numerishe Mathematica*, Vol. 6, 1967, p. 428.

[25]Beam, R. and Warming, R. F., "An Implicit Factored Scheme for Compressible Navier-Stokes Equations," AIAA Paper 77-645, June 1977.

[26]Jameson, A., Schmidt, W., and Turkel, E., "Numerical Solutions of the Euler Equations by Finite Volume Methods Using Runge-Kutta Time-Stepping Schemes," AIAA Paper 81-1259, 1981.

[27]Steger, J. L., "Implicit Finite Difference Simulation of Flow About Arbitrary Two-Dimensional Geometries," *AIAA Journal*, Vol. 16, July 1978, pp. 679–686.

[28]Baldwin, B. S. and Lomax, H., "Thin Layer Approximation and Algebraic Model for Separated Turbulent Flows," AIAA Paper 78-257, Jan. 1978.

[29]Wilson, D. J. and Goldstein, R. J., "Turbulent Wall Jets with Cylindrical Streamwise Surface Curvature," *Journal of Fluids Engineering*, Sept. 1976, pp. 550–557.

[30]Rodi, W. and Scheurer, G., "Calculation of Curved Shear Layers with Two-Equation Turbulence Models," *Physics of Fluids*, Vol. 26, June 1983, pp. 1422–1436.

[31]Thomas, P. D., "Construction of Composite Three-Dimensional Grids from Subregion Grids Generated by Elliptic Systems," *AIAA Journal*, Vol. 20, Sept. 1982, pp. 1195–1202.

[32]Rudy, D. and Strikwerda, J., "A Non-Reflecting Outflow Boundary Condition for Subsonic Navier-Stokes Calculations," *Journal of Computational Physics*, Vol. 36, 1980, pp. 55–70.

[33]Novak, C. J., Cornelius, K. C., and Roads, R. K., "Experimental Investigation of the Circular Wall Jet on a Circulation Control Airfoil," AIAA Paper 87-0155, Jan. 1987.

[34]Englar, R. J. and Williams, R. M., "Test Techniques for High-Lift, Two-Dimensional Airfoils with Boundary Layer and Circulation Control for Application to Rotary Wing Aircraft," NSRDC Rept. 4645, July 1975.